Fermi surface reconstruction in underdoped cuprates

E.A. KOCHETOV
BLTP JINR, DUBNA

Phys. Rev. B 94, 235118 (2016)

Phys. Rev. B 95, 155115 (2017)

arXive: 1706.04011(cond-mat. str-el)

Ilya Ivantsov (BLTP), Alvaro Ferraz (IIP, Brazil), and Evgenii Kochetov

Outline

Introduction: cuprate phase diagram

Itinerant-localized model: cluster perturbation theory

FS reconstruction

Conclusion

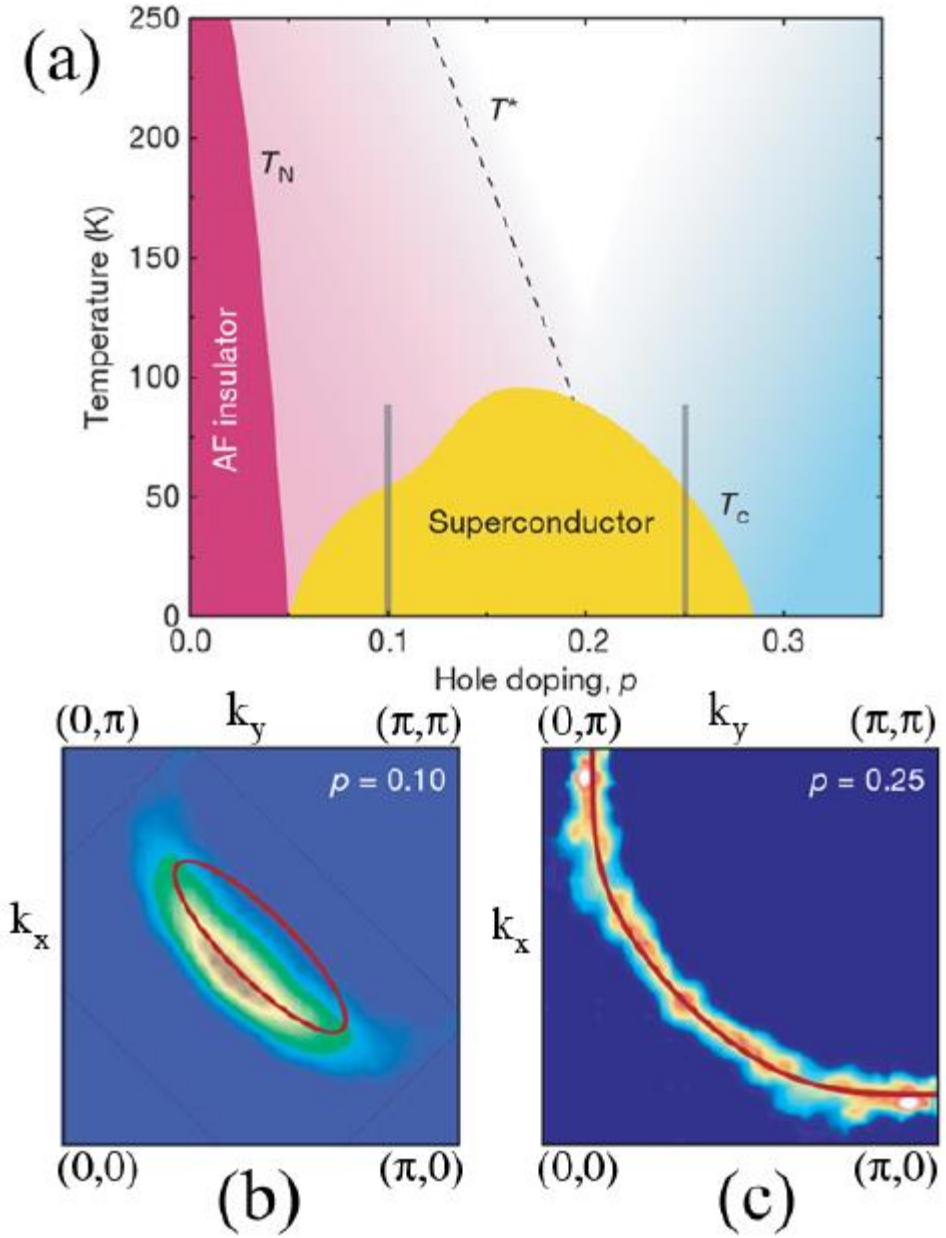
(a)
250
200
150
100
50
0
Temperature (K)
T_N
T^*
AF insulator
Superconductor
T_c
0.0
0.1
0.2
0.3
Hole doping, p
(0,π)
k_y
(π,π)
p = 0.10
k_x
(0,0)
(π,0)
(b)
(0,π)
k_y
(π,π)
p = 0.25
k_x
(0,0)
(π,0)
(c)

Itinerant-localized model

$$H_{t-J} = -\sum_{ij\sigma} t_{ij}\tilde{c}^{\dagger}_{i\sigma}\tilde{c}_{j\sigma} + J\sum_{ij}(\vec{Q}_i \cdot \vec{Q}_j - \frac{1}{4}\tilde{n}_i\tilde{n}_j),$$

$$\tilde{c}^{\dagger}_i = c^{\dagger}_i(1-n_{i-\sigma}) = \frac{1}{\sqrt{2}}(\frac{1}{2} - 2\vec{S}_i \cdot \vec{\sigma})\tilde{d}_i.$$

$$\sum_{\alpha}(\tilde{c}^{\dagger}_{i\alpha}\tilde{c}_{i\alpha}) + \tilde{c}_{i\alpha}\tilde{c}^{\dagger}_{i\alpha} - 1 = \vec{S}_i \cdot \vec{s}_i + \frac{3}{4}(\tilde{d}^{\dagger}_{i\uparrow}\tilde{d}_{i\uparrow} + \tilde{d}^{\dagger}_{i\downarrow}\tilde{d}_{i\downarrow}) = 0,$$

$$\begin{aligned} H_{t-J} &= \sum_{ij\sigma} 2t_{ij}d^{\dagger}_{i\sigma}d_{j\sigma} + J\sum_{ij}(\vec{S}_i \cdot \vec{S}_j) \\ &+ \lambda\sum_i(\vec{S}_i \cdot \vec{s}_i + \frac{3}{4}n^d_i), \quad \lambda/t \gg 1. \end{aligned}$$

FS reconstruction

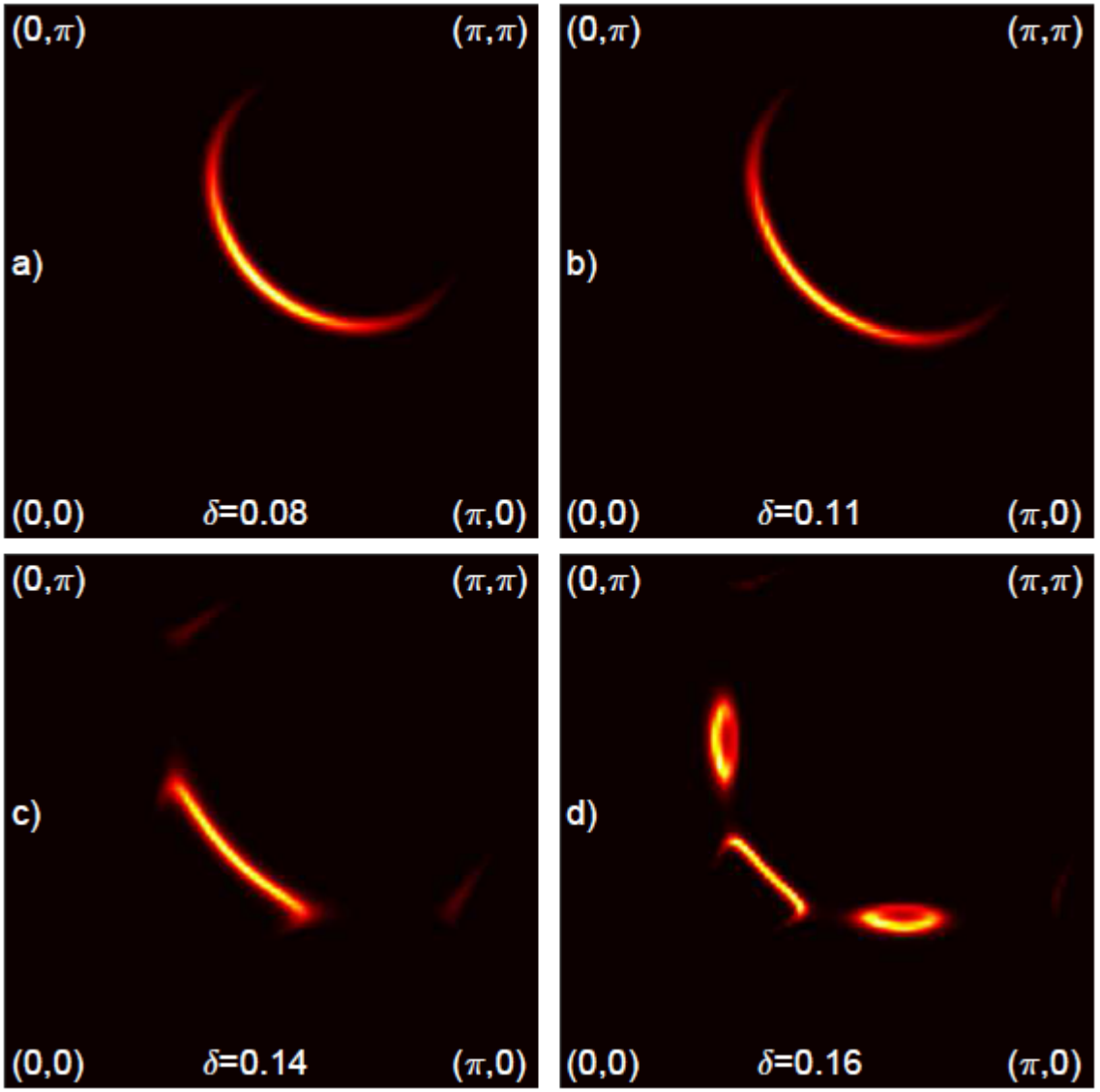

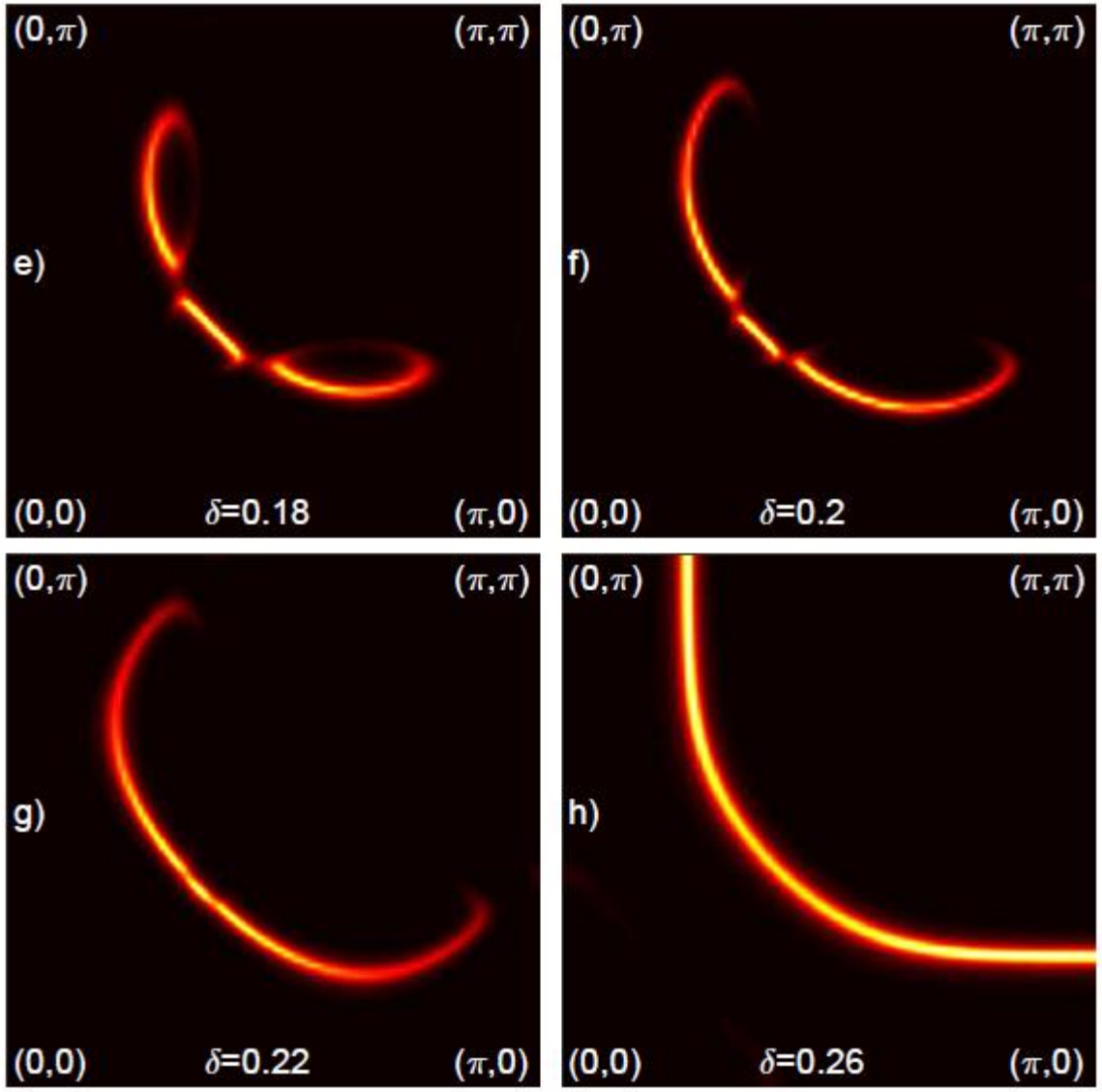
(0,π)
(π,π)
e)
(0,0)
δ=0.18
(π,0)
(0,π)
(π,π)
f)
(0,0)
δ=0.2
(π,0)
(0,π)
(π,π)
g)
(0,0)
δ=0.22
(π,0)
(0,π)
(π,π)
h)
(0,0)
δ=0.26
(π,0)

CDW order

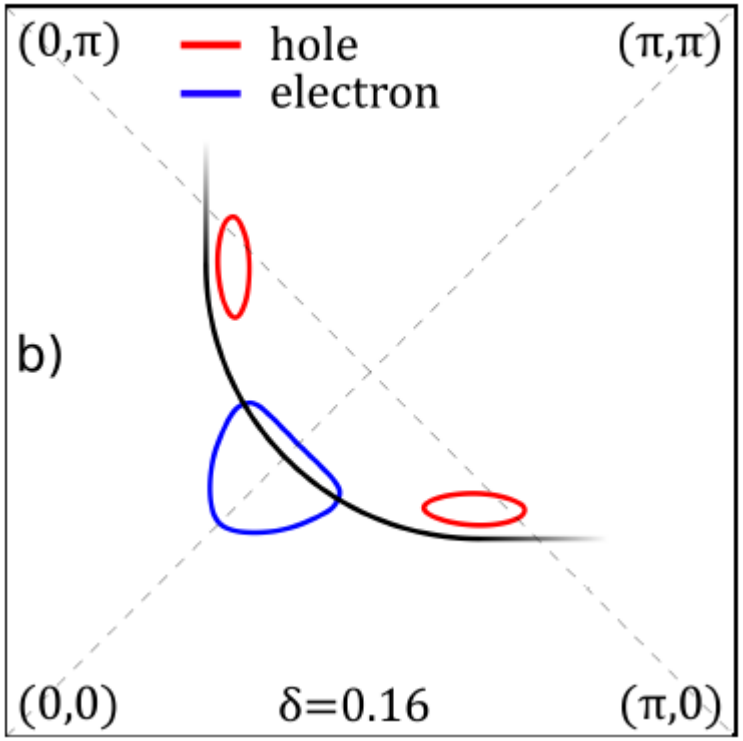

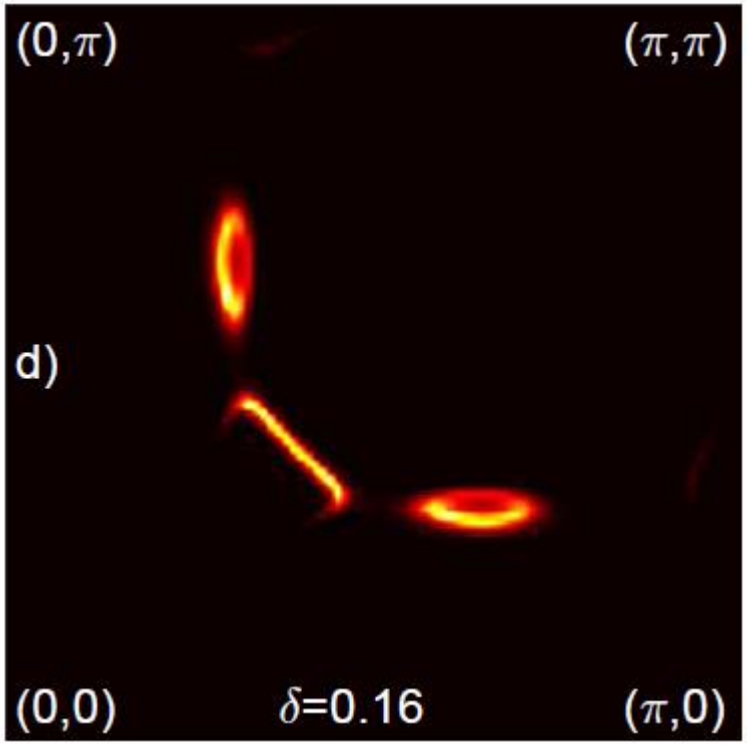

Role of strong electron correlations

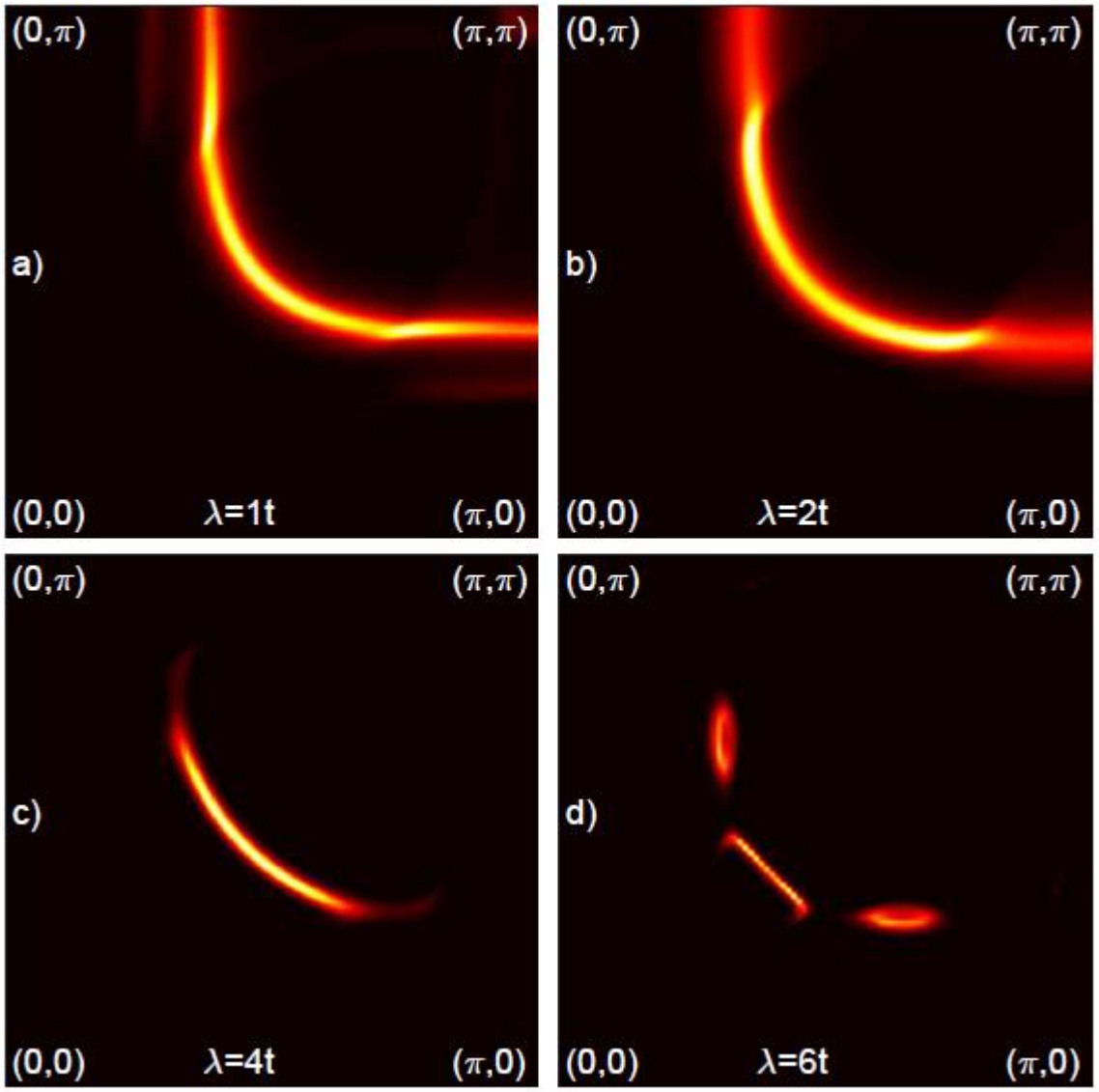

Conclusion

✓Strange metal

✓Charge order and PG phase

Thanks!

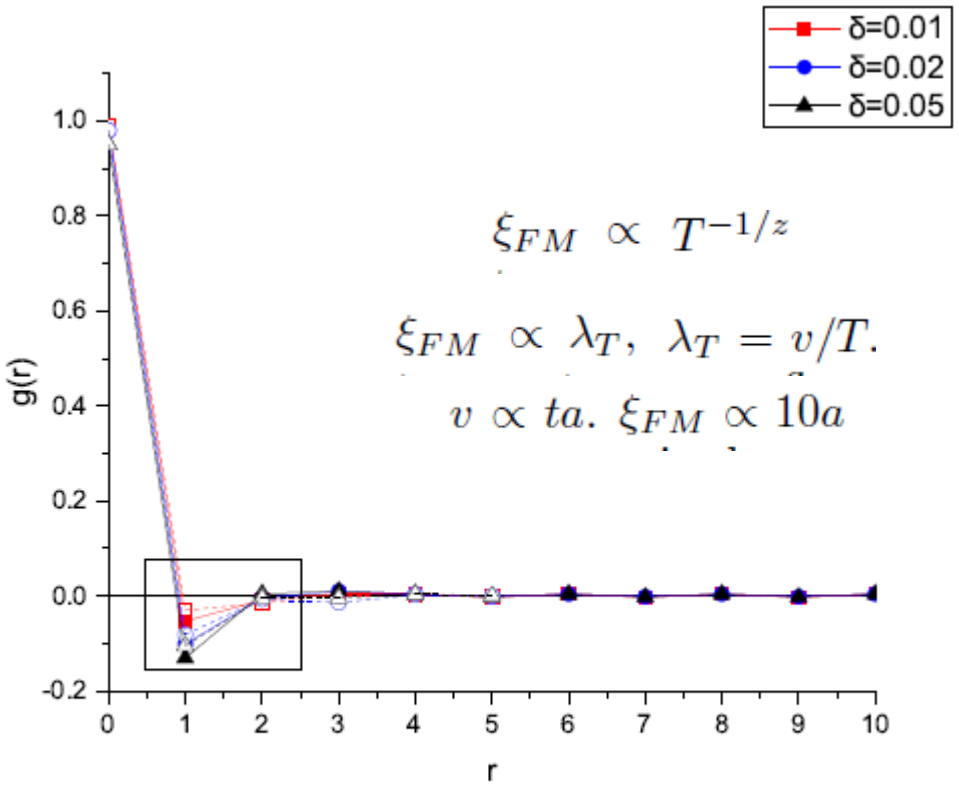

b)

FIG. 4. Panel (a) shows correlation functions for $L = 10$ for different doping levels for the hard-core boson case at $T = 0.1t$. Panel (b) shows the same for fermion case. Solid (dashed) lines show results obtained for $L = 20$ ($L = 10$),

Role of boundary conditions

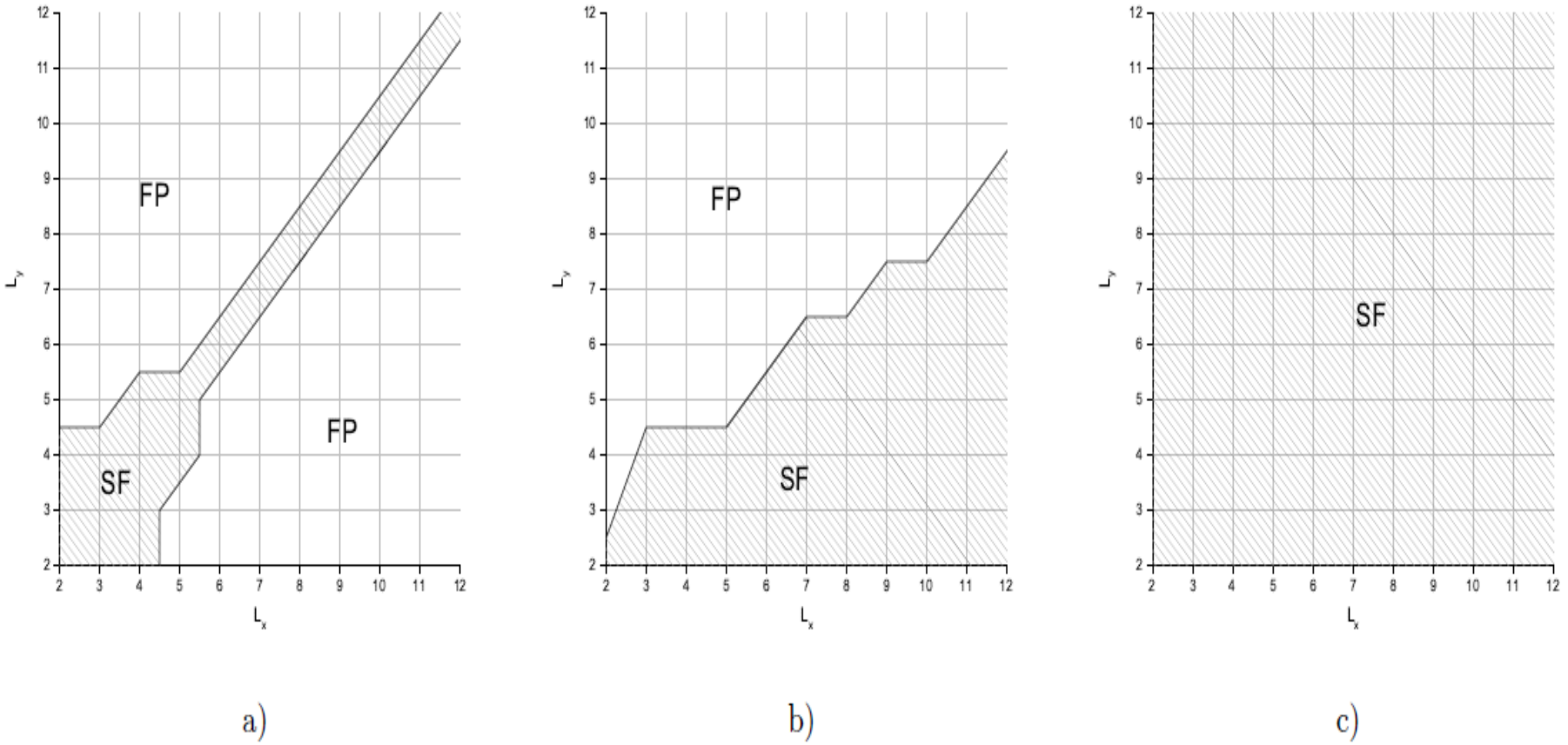

a) b) c)

FIG. 5. The figure shows the energy difference between the fully polarized (FP) state ($Q = Q_{max}$) and the one spin flipped (SF) state ($Q = Q_{max} - 1$)) in case of two holes for the different lattice sizes $N = L_x \times L_y$. The SF areas correspond to the case $E(Q_{max} - 1) < E(Q_{max})$, the FP areas correspond to the case $E(Q_{max} - 1) > E(Q_{max})$. Panel (a) shows the lattice with the open boundary conditions, panel (b) shows the lattice with the periodic boundary condition for the axis x and the open boundary condition for the axis y, panel (a) shows the lattice with the periodic boundary conditions

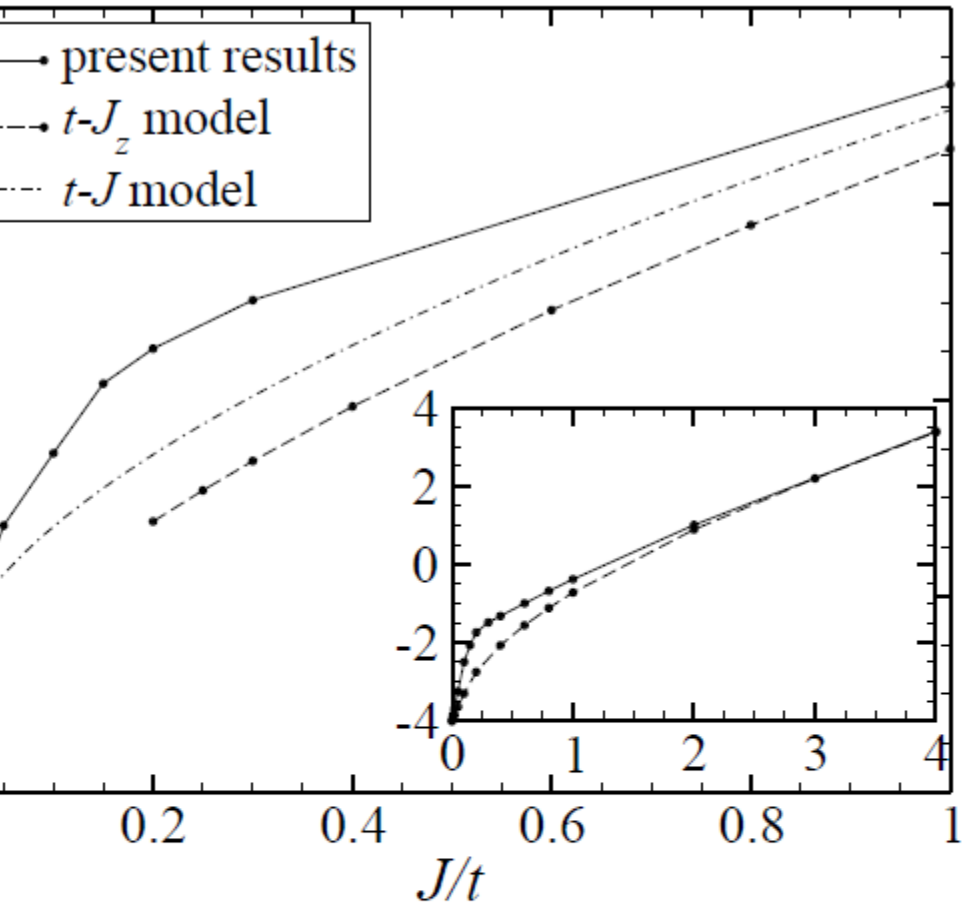

Figure 1. One–hole energy as a function of J/t for a 8×8 cluster at $T =$ data labeled as $t - J_z$ and $t - J$ have been taken from Refs. [29] and [11], respe In the latter case, it is the energy of a hole with momentum $(\pi/2, \pi/2)$. Th shows results obtained for 4×4 $t - J|_{Z_2}$ and t–J_z systems. Here, the dashed lin results presented in Ref. [30] for the t–J_z model. Since for $J \to 0$ the ferrom order sets in, the constraint $\sum_i S_i^z = 0$ is now relaxed.

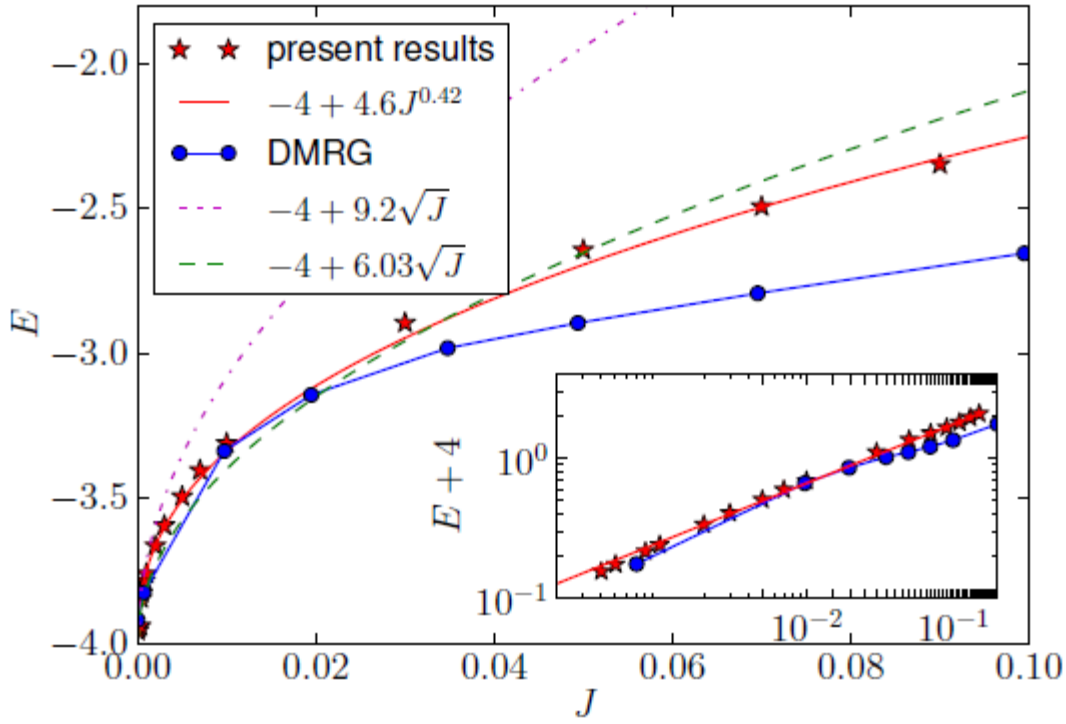

FIG. 2: (Color online) The same as in Fig. 1 but for the energy of a single Nagaoka polaron relatively to the energy of the homogeneous Neel state. The energy is compared with DMRG results for the t–J model taken from Fig. 4 of Ref. 17. The other lines correspond to Eq. (12) for the isotropic t–J (dot-dashed violet line) and a similar expression for the t–J_z model from Ref. 17 (dashed green line). The continuous line shows a power-law fit to the present results.

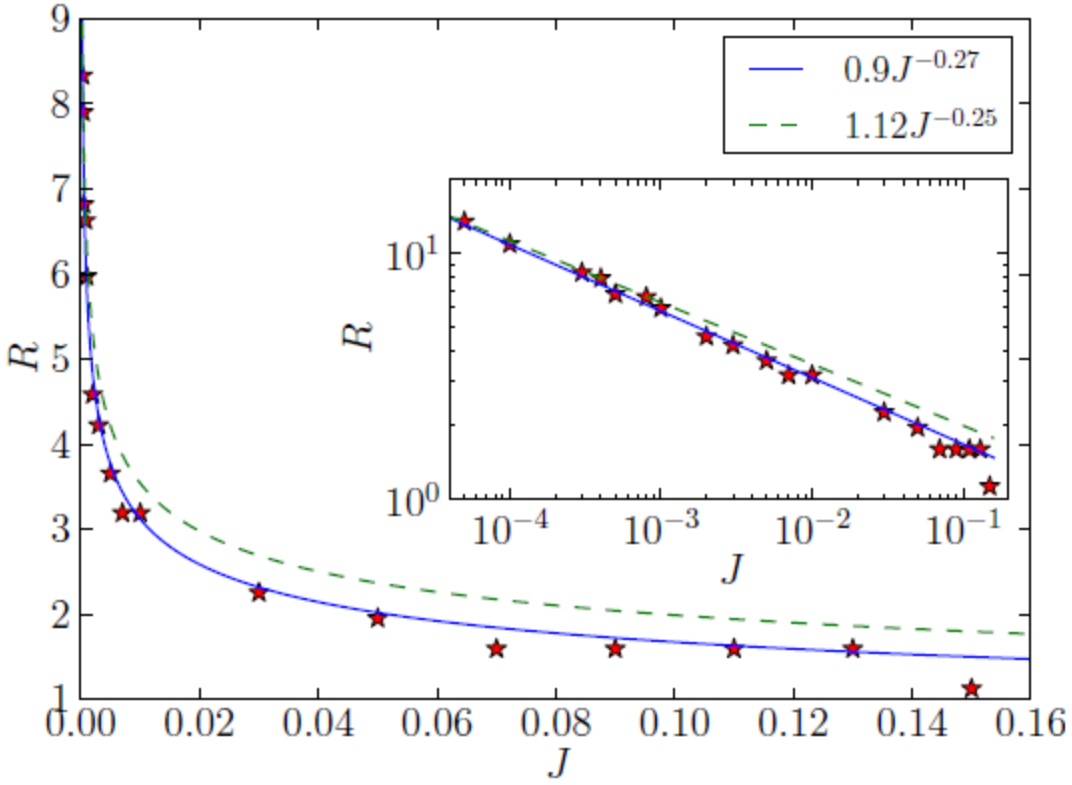

FIG. 1: (Color online) J–dependence of the radius of the Nagaoka polaron formed by a single hole. Points show results from the Monte Carlo calculations for the Ising t–J model, continuous line is the power–law fit and the dashed line shows the dependence described by Eq. (12). Inset shows the same results but on the log–log scale.

No double occupancy constraint and magnetic correlations in cuprates

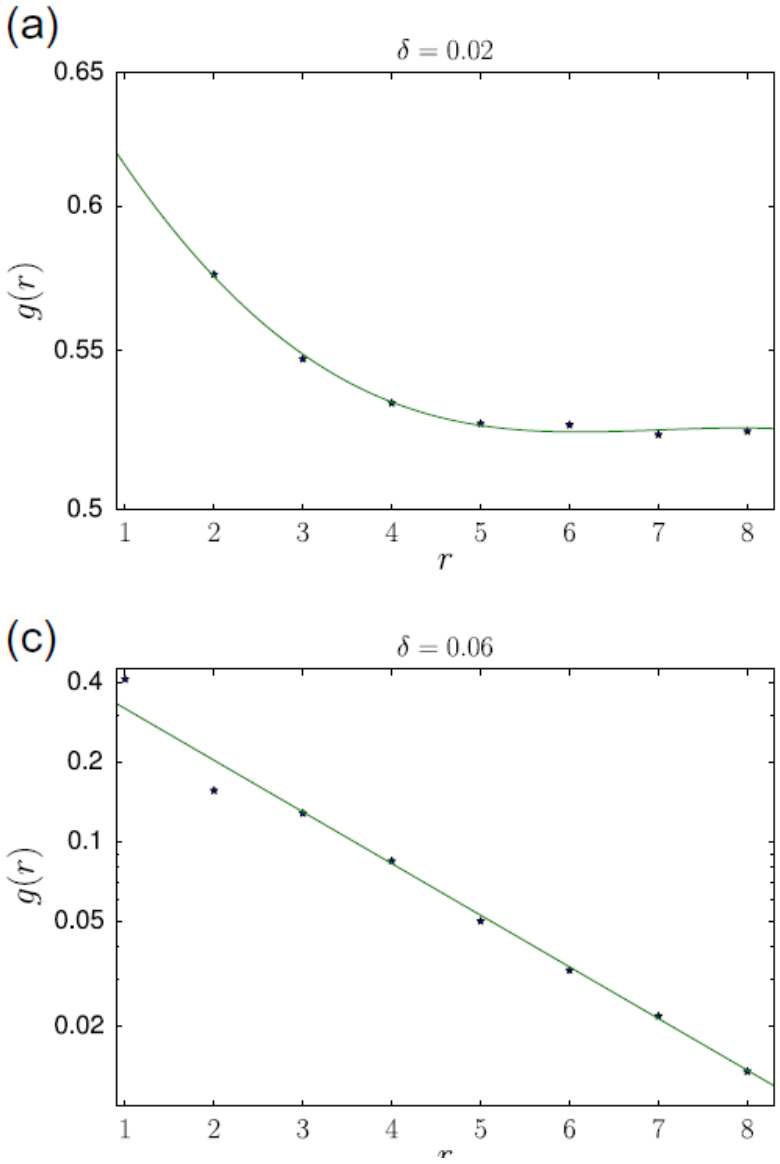

Distance dependence of the spin–spin correlation function $g(r)$ for different hole contrentations δ

The long-range AF order
vanishes at hole concentration below 6 %, which remains in a perfect agreement with experimental data on high-temperatures superconductors. This is very impressive result, as many other techniques give much higher values of concentration, at which AF disappears. The main mechanism responsible for the destruction of the long-range
AF order has its origin in the interplay of the hole mobility and minimization of
the spin-spin exchange
energy.

This strong competition is strictly related to the constraint of no double
occupancy.

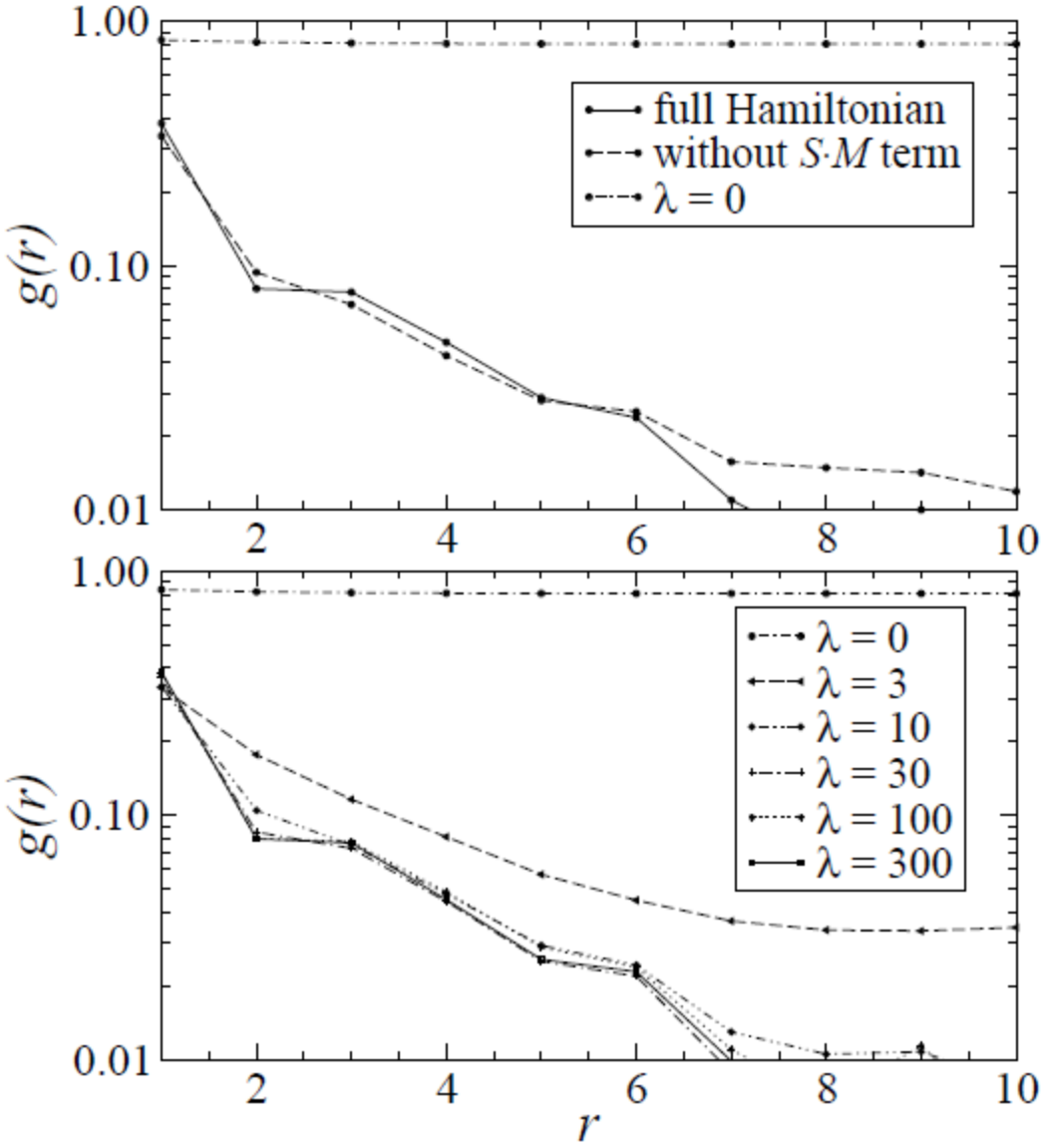

Figure 7. $g(r)$ for $J = 0.2t$, $kT = 0.1t$, $\delta = 0.08$, $t' = -0.27t$ and $t'' = 0.2t$. upper panel the topmost curve has been calculated with $\lambda = 0$. The other curve results obtained for $\lambda = 100t$ with and without the spin–hole exchange interactio lower panel shows $g(r)$ for different values of λ. Note, that the results for λ